NASA CR 159636

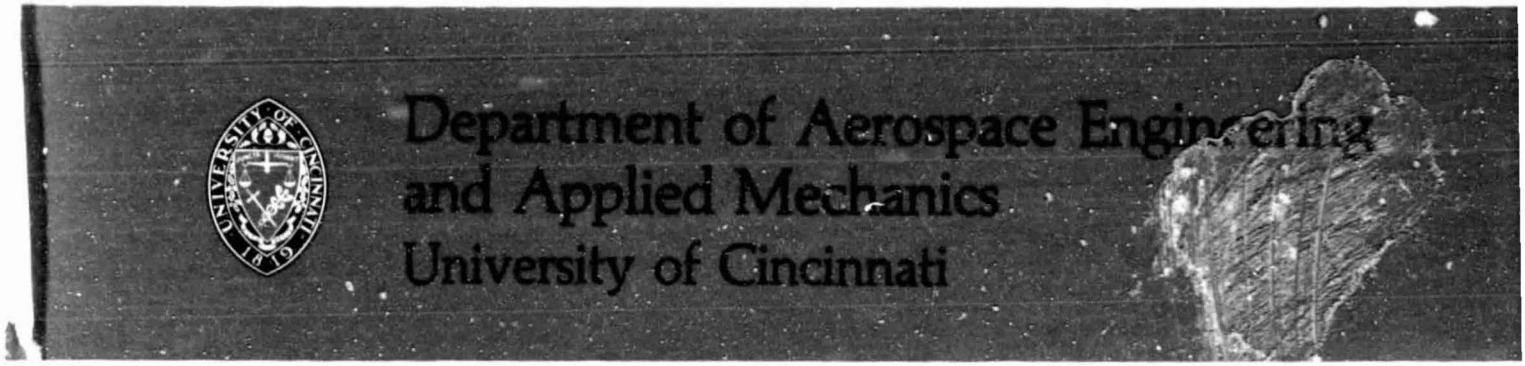

A CALCULATION PROCEDURE FOR VISCOUS FLOW IN TURBOMACHINES - VOL. II

BY

I. KHALIL AND W. TABAKOFF

Supported by:

U.S. Army Research and Technology Laboratories

(AVRADCOM)

Lewis Research Center

Contract No. NAS3-21609

JANUARY 1980

NASA CR 159636

A CALCULATION PROCEDURE FOR VISCOUS FLOW IN TURBOMACHINES - VOL. II

by

I. Khalil and W. Tabakoff

Supported by:

U.S. Army Research and Technology Laboratories

(AVRADCOM)

Lewis Research Center

Contract No. NAS3-21609

JANUARY 1980

TABLE OF CONTENTS

LIST OF TABLES AND FIGURES

SUMMARY

A method for analyzing viscous nonadiabatic flow inside turbomachine passages has been presented earlier in Vol. I of this study. The reported analysis dealt with incompressible laminar flow inside straight radial bladed impellers. In the present volume the developed field analysis is expanded to study turbulent flow within turbomachines having arbitrary blade geometries. Effects of turbulence are modeled using two equations, one expressing the development of the turbulence kinetic energy and the other its dissipation rate. To account for complicated blade geometries, the flow equations are formulated in terms of a nonorthogonal boundary fitted coordinate system.

The analysis is applied to a radial inflow turbine. The solution obtained indicates the severity of the complex interaction mechanism that occurs between the different flow regimes (i.e., boundary layers, recirculating eddies, separation zones, etc.). Comparison with nonviscous flow solutions tend to justify strongly the inadequacy of using the latter with standard boundary layer techniques to obtain viscous flow details within turbomachine rotors. Capabilities and limitations of the present method of analysis are discussed.

The computer used in this work is an AMDAHL 470. The flow domain has been divided into 30 x 40 step sizes. Typical CPU time for the case studied is 520 seconds.

INTRODUCTION

During the last decade extensive progress has been made towards the development of suitable solution methods to the flow in turbomachines. Most of these methods dealt mainly with the flow field inside turbomachines as being inviscid [1, 2]. Few studies, on the other hand, considered viscous effects using some kind of flow approximation [3, 4, 5]. The general flow solutions within turbomachine passages, however, remains mostly beyond the scope of the prevailing modes.

These limitations, especially of the numerical methods, have long been known to be acute due to the complicated nature of the flow problem. The blade rows impose vorticity and velocity fields on the flow. The inviscid effects are dominant,

yet the viscous effects are not small enough to be neglected. Because such flows can only be described using the fully viscous equations of motion, the limitations of the prevailing methods is a direct consequency of at least three major obstacles. The first is the excessive computer time required for the solution of the equation of motion. The second is the difficulties and uncertainties associated with the treatment of certain boundary conditions. The third is the lack of accurate and general methods for describing the turbulent transport phenomena that takes place inside the blade rows.

In an earlier report [7], the authors of this article reported a method suitable for analyzing the viscous incompressible flow in turbomachines that partially overcome the first two obstacles mentioned above. In principle, the approach emphasized the feasibility of obtaining viscous flow details within turbomachine passages by appropriately combining several blade-to-blade viscous flow solutions. Each of these solutions were obtained through the numerical integration of the full Navier-Stokes equations over a predetermined computational surface that extends between the blades. The set of computational surfaces required for the analysis (see Fig. 1) were themselves generated from the solution of the Euler equations in the manner suggested by Wu [1]. The results that had been obtained by applying this method of analysis to flows within straight radial bladed impellers were promising. This was evidenced by the fair agreement achieved between the predicted and experimental data [7].

Recently, the above analysis was extended to deal with nonadiabatic incompressible viscous flows inside turbomachines having arbitrary blade geometries. In particular, the approach which has been established is modified and utilized in conjunction with:

1. A two equation turbulence model.
2. A coordinate transformation package [6] that employs a nonorthogonal boundary-fitted coordinate system to suit the most complicated blade geometries.

The differential equations that describe the viscous flow in turbomachine passages are briefly reviewed in this article with pertinent references made to the questions of their solution efficiency and accuracy of describing the different boundary conditions. The numerical procedures developed on this basis are discussed and illustrated by results obtained for the flow in a cooled radial inflow turbine.

1. MATHEMATICAL FORMULATION

Governing Differential Equations

The development of the mathematical model for the present problem starts with the Reynolds equations for the mean turbulent motion of flow. These equations are written in a generalized form for a turbomachine rotor as follows [7]:

Conservation of Mass:

$$\nabla\cdot(\rho\bar{W}) = 0 \tag{1}$$

Conservation of Momentum:

$$\rho(\bar{W}\cdot\nabla\bar{W} + 2\bar{\Omega} \times \bar{W} - \Omega^2\bar{R})$$

$$= - \nabla p - \nabla\times[\mu_e(\bar{\nabla}\times\bar{W})] + \frac{4}{3}\nabla(\mu_e\nabla\cdot\bar{W}) \tag{2}$$

Conservation of Energy:

$$\rho(\bar{W}\cdot\nabla h) = \frac{\partial p}{\partial t} + (\bar{W}\cdot\nabla)p + D + \nabla\cdot(K\nabla T) \tag{3}$$

where p, ρ, T, h and D denote the static pressure, density, temperature, enthalpy and dissipation function respectively. While, $\bar{W}$ represents the relative velocity vector at any point whose location is defined by the relative position vector $\bar{R}$ in a rotating frame of reference (Fig. 1). The speed of rotation of this frame is equal to the angular velocity of the machine ($\bar{\Omega}$). The effective turbulent viscosity μ_e in the

above equations is assumed to describe the effects of Reynolds stresses and is determined, in the present study, from a two equation turbulence model.

As pointed out in the introduction and elsewhere [7], the flow equations (1) to (3) are solved on several blade-to-blade computational surfaces. The geometry of such surfaces can be conveniently described in terms of the coordinate (m,ϕ,n) as shown in Fig. 1. To reduce the complexity of handling the computations along these surfaces, it is found more convenient [7] to introduce a stream function and the mean vorticity of the turbulent flow as new dependent variables. The flow governing equations (1) through (3), when recasted in terms of these variables and transformed to the (m,ϕ,n) coordinate system result in the following system of equations [7].

Stream Function Equation:

$$\omega = -\frac{1}{r}\left[\frac{\partial}{\partial m}\left(\frac{\dot{M}r}{b\rho}\frac{\partial\psi}{\partial m}\right) + \frac{\partial}{\partial\phi}\left(\frac{\dot{M}}{b\rho r}\frac{\partial\psi}{\partial\phi}\right)\right] \tag{4}$$

In this equation ω denotes the mean vorticity and ψ is the stream function defined according to the following relations:

$$W_m = \frac{\dot{M}}{b}\frac{1}{\rho r}\frac{\partial\psi}{\partial\phi} \quad \text{and} \quad W_\phi = -\frac{\dot{M}}{b}\frac{1}{\rho}\frac{\partial\psi}{\partial m} \tag{4a}$$

where W_m, W_ϕ are the components of the mean relative velocity vector $\bar{W}$ in the meridional, tangential directions, and $\dot{M}$ is the mass flow passing through the volume bounded by the surface S_1 and the filament thickness, b, shown in Fig. 1. The definition of ψ as given by equation (4a) identically satisfies the continuity equation (1). In the process of eliminating the pressure by taking the curl of the momentum equation (2), while using equation (4) and (4a), the following equation is obtained.

Vorticity Transport Equation:

$$\frac{\partial}{\partial m}\left(\frac{\dot{M}}{b}\frac{\partial\psi}{\partial\phi}\omega\right) - \frac{\partial}{\partial\phi}\left(\frac{\dot{M}}{b}\frac{\partial\psi}{\partial m}\omega\right) - \frac{\partial}{\partial m}\left(\mu_e\omega\right)\Big]$$

$$- \frac{\partial}{\partial\phi}\left[\frac{1}{r}\frac{\partial}{\partial\phi}\left(\mu_e\omega\right)\right] + G_1 = 0 \qquad (5)$$

The source term G_1 in the above equation represents the generation or decay of vorticity due to the effects of rotation, it is given by:

$$G_1 = 2\Omega\left[\frac{\partial}{\partial m}\left(\frac{\dot{M}}{b}\sin\alpha\frac{\partial\psi}{\partial\phi}\right) - \frac{\partial}{\partial\phi}\left(\frac{\dot{M}}{b}\sin\alpha\frac{\partial\psi}{\partial m}\right)\right]$$

$$+ \frac{\partial\rho}{\partial m}\frac{\partial W^2/2}{\partial\phi} - \frac{\partial\rho}{\partial\phi}\frac{\partial W^2/2}{\partial m} + \Omega^2 r\sin\alpha\frac{\partial\rho}{\partial\phi}\,. \qquad (5a)$$

Energy Equation:

It is found appropriate for a turbomachine rotor to express the energy equation in terms of the total enthalpy (H) of the flow. The total enthalpy for a turbulent flow is expressed as follows:

$$H = h + \frac{W^2}{2} + \Omega W_\phi r + \frac{\Omega^2 r^2}{2} + E \qquad (6)$$

where E is the kinetic energy of turbulence. Thus, the energy equation (3) when transformed to the (m,ϕ,n) coordinate system, results in [7]:

$$\frac{\dot{M}}{b}\left[\frac{\partial}{\partial m}\left(H\frac{\partial\psi}{\partial\phi}\right) - \frac{\partial}{\partial\phi}\left(H\frac{\partial\psi}{\partial m}\right)\right] - \frac{\partial}{\partial m}\left(\frac{\mu_e}{Pr}r\frac{\partial H}{\partial m}\right) - \frac{1}{r}\frac{\partial}{\partial\phi}\left(\frac{\mu_e}{Pr}\frac{\partial H}{\partial\phi}\right)$$

$$+ \frac{\partial}{\partial m}\left\{\mu_e r\left[\frac{1}{Pr}\frac{\partial W^2/2}{\partial m} - \left(\frac{1}{S_{CE}} - \frac{1}{Pr}\right)\frac{\partial E}{\partial m}\right]\right\}$$

$$+ \frac{\partial}{\partial\phi}\left\{\frac{\mu_e}{r}\left[\frac{1}{Pr}\frac{\partial W^2/2}{\partial\phi} - \left(\frac{1}{S_{CE}} - \frac{1}{Pr}\right)\frac{\partial E}{\partial\phi}\right]\right\}$$

$$- W_\phi\frac{\partial}{\partial m}\left(\mu_e\omega\right) + \frac{W_m}{r}\frac{\partial}{\partial\phi}\left(\mu_e\omega\right) - Dr + G_2 = 0 \qquad (7)$$

where the source term G_2 is given by

$$G_2 = -\Omega \frac{\dot{M}}{b} \{\frac{\partial}{\partial m}[(W_\phi r + r^2\Omega)\frac{\partial \psi}{\partial \phi}] - \frac{\partial}{\partial \phi}[(W_\phi r + r^2\Omega)\frac{\partial \psi}{\partial m}]$$

$$+ \Omega\{\frac{\partial}{\partial m}[\frac{\mu_e}{Pr} r \frac{\partial}{\partial m}(W_\phi r + \frac{\Omega r^2}{2})]$$

$$+ \frac{1}{r}\frac{\partial}{\partial \phi}[\frac{\mu_e}{Pr}\frac{\partial}{\partial \phi}(W_\phi r + \frac{\Omega r^2}{2})]\} \qquad (7a)$$

and the dissipation function, D, is expressed as

$$D = 2\mu_e \{(\frac{\partial W_m}{\partial m})^2 + (\frac{1}{r}\frac{\partial W_\phi}{\partial \phi} + \frac{W_m}{r}\sin\alpha)^2\}$$

$$+ \mu_e \{\frac{\partial W_\phi}{\partial m} + \frac{1}{r}\frac{\partial W_m}{\partial \phi} - \frac{W_\phi}{r}\sin\alpha\}^2 \qquad (7b)$$

In the above equations Pr denotes the turbulent Prandtl number and S_{CE} is the turbulent Schmidt number for the kinetic energy of turbulence E.

Turbulence Model

The mean flow equations introduced earlier as equations (4), (5) and (7) involve more unknowns than appropriate to the equations. This well known problem of closure is a characteristic of all nonlinear stochastic systems. The majority of investigators in the area of turbulent flow have been concerned with this closure problem. The most prominent and practical attempts have been the development of various second order two equation turbulent models. In this, two scalar quantities are used to characterize the turbulence, with each quantity satisfying a nonlinear partial differential equation. Commonly, the two equation models employ the kinetic energy of turbulence as one of the quantities. The second quantity used by different researchers [8] is a dissipation function, a length scale, or a dissipation rate.

The two equation model proposed by Spalding [9] for the kinetic energy of turbulence, E, and its volumetric rate of dissipation ε is used in the present work. Previous experience [10] indicates that this model provides accurate prediction of various flow regimes within turbomachine passages, in addition to being less complex and more general. The complete details of the model and its implications are given in reference [9]; in brief, its main features are outlined in what follows.

The Reynolds stresses are related to the velocity gradients through an effective viscosity, μ_e. This viscosity is assumed to be isotropic at any point, but can vary throughout the flow field. The distribution of the effective viscosity μ_e is determined from the local values of density, ρ, the turbulent kinetic energy, E, and its volumetric dissipation rate, ε. The expression used is:

$$\mu_e = \mu_\ell + C_D \rho \frac{E^2}{\varepsilon} \tag{7c}$$

where the laminar viscosity, μ_ℓ, is considered to be uniform and known.

The equations governing the transport of E and ε have a general form which includes convection, production, diffusion and dissipation terms. These can be written in terms of the (m,ϕ,n) system of coordinates as follows [11].

Turbulent Kinetic Energy Equation:

$$\frac{\dot{M}}{b}\left[\frac{\partial}{\partial m}\left(E\frac{\partial \psi}{\partial \phi}\right) - \frac{\partial}{\partial \phi}\left(E\frac{\partial \psi}{\partial m}\right)\right] - \frac{\partial}{\partial m}\left(\frac{\mu_e}{S_{CE}} r \frac{\partial E}{\partial m}\right)$$

$$- \frac{\partial}{\partial \phi}\left(\frac{\mu_e}{S_{CE}} \frac{\partial E}{r \partial \phi}\right) - rD + \rho \varepsilon r = 0 \tag{8}$$

Dissipation Rate Equation:

$$\frac{\dot{M}}{b}\left[\frac{\partial}{\partial m}\left(\varepsilon\frac{\partial\psi}{\partial\phi}\right)-\frac{\partial}{\partial\phi}\left(\varepsilon\frac{\partial\psi}{\partial m}\right)\right]-\frac{\partial}{\partial m}\left(\frac{\mu_e}{S_{C\varepsilon}}\,r\,\frac{\partial\varepsilon}{\partial m}\right)$$

$$-\frac{\partial}{\partial\phi}\left(\frac{\mu_e}{S_{C\varepsilon}}\,\frac{1}{r}\,\frac{\partial\varepsilon}{\partial\phi}\right)-\bar{C}_1\,\frac{\varepsilon}{E}\,rD+\bar{C}_2\,\frac{\varepsilon^2}{E}\,\rho r=0 \qquad (9)$$

The terms containing the coefficients S_{CE} and $S_{C\varepsilon}$ in equations (8) and (9) represent the diffusion rates of E and ε respectively. These coefficients therefore have the significance of turbulent Schmidt numbers for the transport process in question. The model contains five empirical constants which are assigned the values given in the following table.

Values of the Empirical Constants
for the k-ε Model of Turbulence

C_D	$\bar{C}_1$	$\bar{C}_2$	S_{CE}	$S_{C\varepsilon}$
0.09	1.44	1.92	1.0	1.3

The basis for choosing the above cited constants are discussed in details in reference [9]. It may suffice therefore to remark that $\bar{C}_1$ is chosen so that Von Karman constant equals 0.42 and $\bar{C}_2$ is determined by reference to the decay of grid turbulence. C_D is fixed from the following requirements in a constant stress layer:

$$\tau_w/\rho E = C_D^{1/2} \qquad (9a)$$

where τ_w is the wall shear stress. The diffusion coefficients S_{CE} and $S_{C\varepsilon}$ were fixed in [9] by computer optimization.

It should be emphasized at this point that the additional production of turbulence energy by the rotational effects as well as the effects of surface curvature has been neglected in the present form of the turbulence model. Modifications to include these additional effects continues to be a subject of recent research by different schools.

Equations (4), (5), (7), (8) and (9) are the equations to be solved for ω, ψ, H, E and ε to study the turbomachine flow problem. One can observe that these equations constitute a system of coupled elliptic partial differential equations, involving second order derivatives. From the nature of the problem, none of the terms are negligible in the governing equations. In order to solve these elliptic equations, it is necessary to define a selected region in the physical domain with boundary conditions specified for all the flow variables along the boundaries. The computational domain used is shown in Fig. 2.

Boundary Conditions

Inlet Boundary AN:

Irrotational and prescribed uniform flow conditions are imposed along this boundary. Therefore,

$$\frac{\partial\psi}{\partial m} = -\frac{1}{r}\frac{\partial\psi}{\partial\phi}\tan\beta_{inlet} \quad , \qquad \frac{\partial\psi}{\partial\phi} = \frac{1}{2\pi/z} \quad ,$$

$$\omega = -[2\Omega \sin\alpha]_{inlet} \quad , \qquad H = H_{inlet} \quad . \tag{10}$$

The value of the inelt kinetic energy of turbulence, E_{inlet}, is specified to be 0.05% of the square of inlet velocity.

The dissipation rate is deduced from the turbulence length scale [9]:

$$\varepsilon = E_{inlet}^{3/2} C_D^{3/4}/\ell \tag{10a}$$

where ℓ is taken to be 0.006 m for the case studied in the present work.

The Periodic Boundaries AB, NM and FG, IH:

The periodicity condition is enforced along these boundaries. This implies that the value of all fluid properties as well as their ϕ derivatives, except for the stream function ψ, have equal values at every two corresponding points along AB, NM. Regarding the stream function, the value of ψ's are made to differ on the two boundaries AB, NM by a constant value that is proportional to the mass flow rate, $\dot{M}$. Similarly, the same conditions are imposed along FG, IH.

The Blade Surfaces MI and BF:

A special approach is needed to compute the flow variables near the blade surfaces for the following reasons. In the central region of the flow, the gradients of the flow properties are usually not very steep, and a moderately fine finite difference grid yields accurate solutions. However, close to the blade surfaces, the variations of flow properties are much steeper, thus requiring an extremely fine grid for accurate computation. This implies that the total storage requirement in the computer will be rather large. Moreover, the present form of the turbulence model as given by equations (8) and (9) is valid only for fully turbulent flows. Modifications are required to make it applicable near laminar sublayer regions where the turbulence Reynolds number ($\equiv \rho E^2/\mu_\ell \varepsilon$) is low. To overcome these difficulties, an approach based on the use of wall functions [9] will be employed in the present study. In this approach, all the finite-difference gird nodes (except for those representing the blade surface) are located in the fully turbulent region. It is then assumed that a logarithmic velocity profile exists in the region between the blade surface and the point (w+1) located in the turbulent region. This can be expressed as follows:

$$W_{w+1} = \frac{\dot{M}}{b\rho} \left.\frac{\partial \psi}{\partial N}\right|_{w+1} = C_D^{1/4} E_{w+1}^{1/2} \frac{1}{K} \ell n[e \Delta N \rho C_D^{1/4} E_{w+1}^{1/2}/\mu_\ell] \quad (11)$$

where the subscript (w+1) is used for the values at the internal grid node (w+1), C_D is the constant in the turbulence model,

K and e are the log-wall constants (K = 0.42 and e = 9.0), and ΔN is the distance of (w+1) from the blade surface. The velocity W_{w+1} is assumed to be parallel to the wall-shear stress which is given by:

$$\tau_w = \rho\, C_D^{1/2}\, E_{w+1} \tag{11a}$$

The value of the energy-dissipation rate at the internal grid node ε_{w+1} is determined from the requirement that the length scale varies linearly with the distance from the blade surfaces

$$\varepsilon_{w+1} = \frac{C_D^{3/4}\, E_{w+1}^{3/2}}{K\Delta N} \tag{11b}$$

The value of the energy of turbulence E_{w+1} is calculated from the governing equation (8), with the following modifications. The diffusion of energy to the blade surface is set equal to zero, and the generation term D in equation (8) is modified to account for the value of the wall shear stress as given by equation (11a). The dissipation term is also modified according to equation (11b), and is assigned an average value for the near-wall node as follows:

$$\rho\bar{\varepsilon} = \rho \int_0^{N_{w+1}} \varepsilon dN = \rho\, C_D^{3/4}\, E_{w+1}^{3/2} \int_0^{N_{w+1}} \frac{1}{KN}\, dN \tag{11c}$$

For the vorticity boundary condition, equation (11) is used in conjunction with the stream function equation (4) to determine ω at the grid node (w+1).

Downstream Boundary GH:

The conditions of zero gradients in the meridional direction are imposed along this boundary for H, E and ε, i.e.

$$\frac{\partial H}{\partial m} = 0 \tag{12}$$

and

$$\frac{\partial E}{\partial m} = \frac{\partial \varepsilon}{\partial m} = 0 \tag{12a}$$

For the vorticity ω, the absolute value is taken to be zero, thus

$$\omega = - [2\Omega \sin\alpha]_{exit} \tag{12b}$$

For the stream function ψ, the downstream flow velocities, which may be used to determine ψ derivatives along GH, and that guarantee a unique solution to the problem are unknow apriori. Therefore, a supplementary condition based on the conservation of angular momentum principle is employed in the present work to yield the required unique solution. The details of the procedure can be found in reference [7].

Coordinate Transformation

The solution of equations (4)-(9) subjected to the appropriate boundary conditions discussed earlier are carried out numerically. In order to reduce the complexity of handling the numerics near the curved boundaries of the blade surface, a coordinate transformation of the (m,ϕ,n) system to a contracted boundary fitted coordinate is required. The overall effect of this transformation is to produce a square field in which the blade surfaces become straight and parallel. As pointed out earlier in reference [7], two transformations are used to implement the generation of the boundary fitted coordinates for the blade-to-blade domain in Fig. 3a. The first one is obtained by defining a stretched meridional coordinate, x, given by:

$$dx = \frac{dm}{r} \tag{13a}$$

The second transformation [6] generates the boundary fitted coordinates ξ and η through the numerical solution of the following equations for $x(\xi,\eta)$ and $\phi(\xi,\eta)$.

$$\alpha \frac{\partial^2 x}{\partial \xi^2} - 2\beta \frac{\partial^2 x}{\partial \xi \partial \eta} + \gamma \frac{\partial^2 x}{\partial \eta^2} = Q(\xi,\eta)$$

$$\alpha \frac{\partial^2 \phi}{\partial \xi^2} - 2\beta \frac{\partial^2 \phi}{\partial \xi \partial \eta} + \gamma \frac{\partial^2 \phi}{\partial \eta^2} = P(\xi,\eta) \tag{13b}$$

where

$$\delta = \left(\frac{\partial x}{\partial \eta}\right)^2 + \left(\frac{\partial \phi}{\partial \eta}\right)^2 \quad , \quad \beta = \frac{\partial x}{\partial \eta}\frac{\partial x}{\partial \xi} + \frac{\partial \phi}{\partial \xi}\frac{\partial \phi}{\partial \eta} \quad ,$$

$$\gamma = \left(\frac{\partial x}{\partial \xi}\right)^2 + \left(\frac{\partial \phi}{\partial \xi}\right)^2 \quad . \tag{13c}$$

The functions Q and P in the above equations are appropriately chosen to provide control over the spacing of the coordinate lines in the field.

Mapping the region of interest in Fig. 3a in terms of the new boundary-fitted system of coordinates (ξ,η) yields a fixed square field in the final transformed domain as shown in Fig. 3b. Thus, it is possible to carry out all flow calculations on the fixed square field, using uniform grid with no interpolation required regardless of the blades shape in the physical space.

Before transforming the flow equations (4)-(9) from the physical domain to the fixed square field, it is found convenient to express the flow variables in these equations in the following dimensionless form:

$$\omega^* = \frac{\omega r_t}{(W_m)_o} \quad , \quad H^* = \frac{H}{(W_m^2)_o} \quad , \quad r^* = \frac{r}{r_t} \quad , \quad b^* = \frac{b}{b_t} \quad ,$$

$$E^* = \frac{E}{(W_m^2)_o} \quad , \quad \varepsilon^* = \frac{\varepsilon r_t}{(W_m^3)_o} \quad , \quad Re = (W_m)_o \frac{\rho r_t}{\mu_e} \quad , \quad R_o = \frac{\rho \Omega r_t^2}{\mu_e} \tag{14}$$

where the subscripts o, t denotes the conditions at the upstream boundaries (A-N) and (M-B) respectively.

By applying the chain rule for partial differentiation and using the expressions given by the relation (14), the governing flow equations in the transformed domain can be written in terms of the new variables (ξ,η) as [7]:

Stream Function Equation:

$$\frac{r_o}{r_t}\frac{b_o}{b_t}\frac{2\pi}{z}\left\{\alpha\frac{\partial}{\partial\xi}\left(\frac{1}{b^*}\frac{\partial\psi}{\partial\xi}\right)+\gamma\frac{\partial}{\partial\eta}\left(\frac{1}{b^*}\frac{\partial\psi}{\partial\eta}\right)-\beta\frac{\partial}{\partial\xi}\left(\frac{1}{b^*}\frac{\partial\psi}{\partial\eta}\right)\right.$$

$$\left.-\beta\frac{\partial}{\partial\eta}\left(\frac{1}{b^*}\frac{\partial\psi}{\partial\xi}\right)\right\}=-\omega^*\,r^{*2}J^2 \qquad (14)$$

Vorticity Transport Equation:

$$J\left[\frac{\partial}{\partial\xi}\left(\frac{\omega^*}{b^*}\frac{\partial\psi}{\partial\eta}\right)-\frac{\partial}{\partial\eta}\left(\frac{\omega^*}{b^*}\frac{\partial\psi}{\partial\xi}\right)\right]+2J\frac{R_o}{Re}\left[\frac{\partial}{\partial\xi}\left(\frac{\sin\alpha}{b^*}\frac{\partial\psi}{\partial\eta}\right)\right.$$

$$\left.-\frac{\partial}{\partial\eta}\left(\frac{\sin\alpha}{b^*}\frac{\partial\psi}{\partial\xi}\right)\right]-\frac{r_t}{r_o}\frac{b_t}{b_o}\frac{z}{2\pi}\left[\delta\frac{\partial^2}{\partial\xi^2}\left(\frac{\omega^*}{Re}\right)\right.$$

$$\left.+\gamma\frac{\partial^2}{\partial\xi^2}\left(\frac{\omega^*}{Re}\right)-2\beta\frac{\partial^2}{\partial\xi\partial\eta}\left(\frac{\omega^*}{Re}\right)\right]=0 \qquad (15)$$

Energy Equation:

$$J\frac{b_o^*}{b^*}\left[\frac{\partial}{\partial\xi}\left(H^*\frac{\partial\psi}{\partial\eta}\right)-\frac{\partial}{\partial\eta}\left(H^*\frac{\partial\psi}{\partial\xi}\right)\right]-\frac{r_t}{r_o}\frac{Z}{2\pi}\left[\delta\frac{\partial}{\partial\xi}\left(\frac{1}{Re}\frac{1}{Pr}\frac{\partial H^*}{\partial\xi}\right)\right.$$

$$-\beta\frac{\partial}{\partial\xi}\left(\frac{1}{Re}\frac{1}{Pr}\frac{\partial H^*}{\partial\eta}\right)-\beta\frac{\partial}{\partial\eta}\left(\frac{1}{Re}\frac{1}{Pr}\frac{\partial H^*}{\partial\xi}\right)$$

$$\left.+\gamma\frac{\partial}{\partial\eta}\left(\frac{1}{Re}\frac{1}{Pr}\frac{\partial H}{\partial\eta}\right)-D^*+G_4^*\right]=0 \qquad (16)$$

Turbulent Kinetic Energy Equation:

$$J \frac{b_o^*}{b^*} \left[\frac{\partial}{\partial \xi}\left(E^* \frac{\partial \psi}{\partial \eta}\right) - \frac{\partial}{\partial \eta}\left(E^* \frac{\partial \psi}{\partial \xi}\right)\right] - \frac{r_t}{r_o} \frac{z}{2\pi} \left[\delta \frac{\partial}{\partial \xi}\left(\frac{1}{Re} \frac{1}{S_{CE}} \frac{\partial E^*}{\partial \xi}\right)\right.$$

$$- \beta \frac{\partial}{\partial \xi}\left(\frac{1}{Re} \frac{1}{S_{CE}} \frac{\partial E^*}{\partial \eta}\right) - \beta \frac{\partial}{\partial \eta}\left(\frac{1}{Re} \frac{1}{S_{CE}} \frac{\partial E^*}{\partial \xi}\right)$$

$$\left. + \gamma \frac{\partial}{\partial \eta}\left(\frac{1}{Re} \frac{1}{S_{CE}} \frac{\partial E^*}{\partial \eta}\right)\right] - D^* + \frac{z}{2\pi} J^2 \varepsilon^* \frac{r^{*2}}{r_o} = 0 \qquad (17)$$

Dissipation Rate Equation:

$$J \frac{b_o^*}{b^*} \left[\frac{\partial}{\partial \xi}\left(\varepsilon^* \frac{\partial \psi}{\partial \eta}\right) - \frac{\partial}{\partial \eta}\left(\varepsilon^* \frac{\partial \psi}{\partial \xi}\right)\right] - \frac{r_t}{r_o} \frac{z}{2\pi} \left[\delta \frac{\partial}{\partial \xi}\left(\frac{1}{Re} \frac{1}{S_{C\varepsilon}} \frac{\partial \varepsilon^*}{\partial \xi}\right)\right.$$

$$- \beta \frac{\partial}{\partial \xi}\left(\frac{1}{Re} \frac{1}{S_{C\varepsilon}} \frac{\partial \varepsilon^*}{\partial \eta}\right) - \beta \frac{\partial}{\partial \eta}\left(\frac{1}{Re} \frac{1}{S_{C\varepsilon}} \frac{\partial \varepsilon^*}{\partial \xi}\right)$$

$$\left. + \gamma \frac{\partial}{\partial \eta}\left(\frac{1}{Re} \frac{1}{S_{C\varepsilon}} \frac{\partial \varepsilon^*}{\partial \eta}\right)\right] - \bar{C}_1 D^* \frac{\varepsilon^*}{E^*} + \frac{z}{2\pi} \bar{C}_2 J^2 \frac{\varepsilon^{*2}}{E^*} \frac{r^{*2}}{r_o}$$

$$= 0 \qquad (18)$$

where z is the number of blades, D^* and G_4^* are the nondimensional equivalent of the source terms D and G_2 in equations (7b) and (7a). The transformation parameters, J, δ, β, γ in the above equations are defined, in the present work, using Thompson's numerical package [6].

As pointed out in reference [7], the solution of equations (14)-(18) in the (ξ,η) domain provides the required distribution of the flow variables ψ, ω, H, E and ε in the physical space. In order to solve these equations numerically, a suitable finite difference method is required. The computational method used is outlined in the following section.

2. SOLUTION PROCEDURES

The derivation of the general finite difference equations corresponding to equations (14)-(18) is described first. This is followed by the procedures employed for the simultaneous solution of the resulting difference equations.

Referring to Fig. 3b, the finite difference representation of equations (14)-(18) is obtained using standard five point difference operator. Thus,

$$\psi_{i,j} = A_1\psi_{i+1,j} + A_2\psi_{i-1,j} + A_3\psi_{i,j+1} + A_4\psi_{i,j-1} + A_5 \quad , \tag{19}$$

$$\omega^*_{i,j} = B_1\omega^*_{i+1,j} + B_2\omega^*_{i-1,j} + B_3\omega^*_{i,j+1} + B_4\omega^*_{i,j-1} + B_5 \quad , \tag{20}$$

$$H^*_{i,j} = C_1H^*_{i+1,j} + C_2H^*_{i-1,j} + C_3H^*_{i,j+1} + C_4H^*_{i,j-1} + C_5 \quad , \tag{21}$$

$$E^*_{i,j} = D_1E^*_{i+1,j} + D_2E^*_{i-1,j} + D_3E^*_{i,j+1} + D_4E^*_{i,j-1} + D_5 \quad , \tag{22}$$

and

$$\varepsilon^*_{i,j} = K_1\varepsilon^*_{i+1,j} + K_2\varepsilon^*_{i-1,j} + K_3\varepsilon^*_{i,j+1} + K_4\varepsilon^*_{i,j-1} + K_5 \tag{23}$$

where the value of the different coefficients in the above equations are given in Table 1. A combination of central and upwind differences are used for evaluating these coefficients. The details of the differencing techniques is reported in reference [7].

Solution of equations (19)-(23) will be obtained using a successive relaxation iterative method. In using this method there are alternate methods for handling the coupling between the governing equations. For example, if these equations are solved in sequence, the coupling has to be restored through repeated iterations. Not all iterative schemes, however converge to a solution and experience proves that the solution of a system of coupled nonlinear equations converges for laminar flows, but diverges for turbulent flows. The problem of instability usually arises from the coupling between the mean velocity profile and effective viscosity profile. Reference [12] suggests the use of a successive convergence technique to retard and dampen this coupling to ensure convergence under any set of boundary conditions.

The successive convergence technique is implemented in the present work by decoupling the turbulent kinetic energy and dissipation rate equations (22) and (23) from the remaining equations. The former are solved sequentially rather than simultaneously with the vorticity and the stream function equations (19) and (20). The details of the procedure is as follows. The stream function and vorticity equations are first solved with a frozen viscosity field using the same numerical scheme outlined previously in reference [7]. Once a convergence solution has been obtained, the kinetic energy of turbulence and the dissipation rate equations are then solved using a Gauss-Siedel method to obtain a new round of frozen viscosity field which will be used in the next cycle of convergent solution for ψ, ω. The step described immediately above is executed several times until a convergence criteria is satisfied. When the calculations have reached this stage, the energy equation (21) is then solved using again the Gauss-Siedel method.

The computer program used to carry out the actual flow calculations is an expanded version of the one used in Part I

of this study. In order to keep the computer time within reasonable limits (usually less than nine minutes for turbulent cases on an AMDAHL 470), the unit square region has been divided into 30 step sizes in η direction and 40 in the ξ direction. These grids have not been optimized, however they will suffice for the present purpose, which is to demonstrate the capability of carrying out calculations of this type of flow.

3. COMMENTS ON THE COMPUTATIONAL METHOD

Before proceeding to a detailed discussion of the numerical solution of the flow case studied, a few comments are given first.

Special consideration had to be taken into account during the numerical generation of the boundary fitted coordinate system for the blade-to-blade domain of Fig. 3. This pertained to the enforcement of the periodic boundary conditions in an effective manner. In order not to resort to additional iterations solely for the purpose of enforcing the periodicity conditions, it was required that the ξ coordinate line emanating from one point on the lower boundary AB of Fig. 3 must meet the upper boundary NM at the point having the same meridional location. Generally, this constraint was easily satisfied, since as explained in reference [7], the assignment of the ξ-values to the boundary points via the functions f_1, f_2, g_1 and g_2 is arbitrary. Although the distribution in the ξ lines, in these cases, did not necessarily produce orthogonal coordinates, as exemplified in Fig. 3, the lack of orthogonality created no problem at all.

Some problems arose with the convergence characteristics of the kinetic energy of turbulence equation during the numerical solutions. Guided by an analysis, for a simple test case with

few grid points, and by subsequent experience on the computer, the cause of the problem was traced and defined to be the source term (D) in equation (3). Since this term is a function of the square of the kinetic energy itself [see equations (7b) and (7c)], it might therefore be anticipated that this term vary so widely, during the iteration procedure, so as to provoke divergence. To reduce these variations, a rearrangement of the finite difference equation (22) is sought. For this the source term, D, was written as

$$D = \mu_e F_1 = \mu_\ell F_1 + E \{C_D \rho \frac{E}{\varepsilon} F_1\} \tag{24a}$$

where

$$F_1 = 2[(\frac{\partial W_m}{\partial m})^2 + (\frac{1}{r}\frac{\partial W_\phi}{\partial \phi} + \frac{W_m}{r}\sin\alpha)^2]$$

$$+ (\frac{\partial W_\phi}{\partial m} + \frac{1}{r}\frac{\partial W_m}{\partial \phi} - \frac{W_\phi}{r}\sin\alpha)^2 \tag{24b}$$

Thus, by substituting equation (24a) in equation (22), and rearranging, one obtains:

$$E^*_{i,j} = \frac{D_1 E^*_{i+1,j} + D_2 E^*_{i-1,j} + D_3 E^*_{i,j+1} + D_4 E^*_{i,j-1} + \bar{D}_5}{(1 + \omega_E \Delta\eta\, C_D\, F_1^* E^*/\varepsilon^*/D_o)_{i,j}} \tag{24c}$$

where

$$\bar{D}_5 = \Delta\xi\,\Delta\eta\,[-\mu_\ell F_1^* + \frac{2\pi}{z} J^2 \varepsilon^* \frac{r^{*2}}{r_o} - \beta \frac{\partial}{\partial\xi}(\frac{1}{Re}\frac{1}{S_{CE}}\frac{\partial E^*}{\partial\eta})$$

$$- \beta \frac{\partial}{\partial\eta}(\frac{1}{Re}\frac{1}{S_{CE}}\frac{\partial E^*}{\partial\xi})]/D_o \tag{24d}$$

With this new substitution formula, the variations in the modified source term was found to be much less than those of the original one and convergence was restored for all cases studied in the present work.

A problem similar to that immediately discussed above was developed with the source term in the dissipation rate equation (18). Again, the finite difference equation (23) was rearranged in a similar manner so as to dampen the variation of the source during the numerical solution.

It is appropriate to mention at this stage a special practice was employed near the blade exit region along the boundary FI (see Fig. 2). Under certain circumstances, a smooth variation for the kinetic energy of turbulence and its dissipation rate, was not achievable near the blade exit. This in turn caused some difficulties in the calculations, and eventually induced divergence especially in cases involving small convergence criteria. In order to alleviate this kind of restriction, the condition given by equation (12a) was applied along the boundary FI in Fig. 2 instead of the boundary HG. Although this modification ensured convergence, under any set of conditions, it is felt that further study is recommended to remove the inadequacy resulting from the neglect of the decay of E and ε downstream the blade row.

The calculation procedures used to establish convergence for each cycle of solution for the stream function and vorticity were covered in some detail in Volume I of this study [7]. Typically, intermediate convergent solutions at given effective viscosity distributions were obtained after 50-80 iterations on the average. A succession of 15-25 rounds of intermediate convergent solutions with frozen effective viscosity fields were required for a complete numerical solution of a typical problem. In the case studied here, the determining convergence criteria, in each cycle of ω and ψ calculations, turned out to be the vorticity tolerance. That is, when the vorticity tolerance was finally satisfied, the stream function error was considerably below the required values. Likewise, the determining convergence criteria during the subcycle of E and ε calculations turned out to be the kinetic energy of turbulence tolerance.

4. RESULTS AND DISCUSSION

The procedure described in the previous sections is employed to obtain the flow details in a cooled radial inflow turbine rotor. The rotor geometry is shown in Fig. 4 together with the shape and thickness distribution of the computational surface S_1. The blade-to-blade shape in the physical domain as well as the boundary fitted coordinates employed in the solution are those shown in Fig. 3. Additional summary data related to the blades geometry and the configuration of the computational surface S_1 can be found in Table 2. The following operating conditions for the turbine are used in the analysis:

Turbine inlet total temperature, T_t, 1083°K

Turbine inlet density, ρ, 1.0060 Kg/m^3

Rotational speed, Ω, 38,500 r.p.m.

Rotor inlet flow angle, β_{in}, 62.5°

Rotor exit flow angle, β_{exit}, 63°

Meridional component of the relative velocity at rotor inlet, W_m, 66.2 m/s

Flow Reynolds number at rotor inlet, $Re \left(\equiv \frac{\rho W_m r_{tip}}{\mu_e}\right)_{inlet}$, 3.34×10^5

Prandtl number, 0.8

The flow through the turbine is considered to be incompressible and the blade surfaces are cooled and kept at a uniform temperature of 550°K.

Results of the analysis are presented in Figs. 5 through 9 as contour plots for the distribution of the stream function, the velocity, the kinetic energy of turbulence as well as the temperature within the blade passages.

The stream function contour plots are given in Fig. 5. The flow contours depicted reflect the appearance of a recirculating eddy near the pressure surface of the blades. The flow rate within the eddy amounts to about 2.5% of the flow rate through the turbine (as indicated by the designation of the streamlines). This low flow rate implies low relative velocities within the eddy as will be discussed shortly. The manner in

which the streamline ($\psi = 1$) leaves the blade surface indicates that a separation bubble is formed over the aft portion of the blade suction surface. This behavior seemed to be caused by the inability of the flow to accommodate the large blade deflection angle in this region.

The distribution of relative velocity, W, across the blade-to-blade passage, nondimensionalized with respect to the blade tip speed, Ωr_{tip}, is shown in Fig. 6. The contours show a core of high relative velocity centered at a point located at approximately 15 percent of the passage width from the blade suction surface. A region of distinct velocity deficiency is also observed in the upper half of the passage extending to about 70 percent the blade chord and is most pronounced near the blade pressure surface. This region coincides with the location of the recirculatory eddy shown in Fig. 5. The data in Fig. 6 also indicates that the flow experiences a high acceleration rate near the blade pressure surface as it approaches the passage exit. This behavior is similar to that of flow approaching a turning duct and is expected.

In order to gain some insight into the development of the boundary layer over the blade surfaces, the velocity profiles, across the rotor passage, at different meridional locations are introduced in Fig. 7. The locations are selected to correspond to the meridional distances 1.0, 4.0 and 6.0 cms respectively. The profiles of Fig. 7a and 7b show reversed flow regions existing near the blade pressure surface and steep gradients in the velocity near the suction surface. There is a noticeable change in the velocity profiles at subsequent downstream stations. A jet type of profile exists near the turbine exit as illustrated in Fig. 7c. The complex flow pattern observed generally in Figs. 6 and 7 indicates the significant extent of the complex interaction mechanism that occurs between the different flow regimes (i.e. boundary layers, recirculating eddies and separation regions, etc.) within the rotor channel. As a consequency of such interaction, no clear distinction can be

made between the boundary layer regions and the inviscid core. This result emphasizes the inaccuracies involved in using a nonviscous flow solution, such as the one shown in Fig. 7 (with dotted lines), to generate boundary layer characteristic parameters for flows in turbomachine rotors.

Figure 8 shows the distribution of the kinetic energy of turbulence between the blades. The turbulence intensities are plotted using the nondimensional quantity $E' = E/\Omega^2 r_{tip}^2$. Near the passage inlet and up to 60 percent of the blade chord peak turbulence intensities are observed to occur in the mixing region of the recirculating eddy noted in Fig. 5. The flow energy dissipated in this process of recirculation is responsible for the velocity defficiency encountered near the blade pressure surface as shown in Fig. 5. On the whole, it could be recognized that the turbulence intensities are generally higher than those encountered in a stationary passage. The maximum intensities are seen to occur near the blade surfaces and especially at the passage exit. The relatively high values of kinetic energy of turbulence shown in the figure away from the blade surfaces reflect the extent of turbulent mixing even near the mid passage. The classical assumption that the viscous and turbulence effects are confined to very thin regions near the blade surfaces is evidently inaccurate when dealing with flow in turbomachinery. It is with the present type of analysis that involves the solution of the full field equations in addition to a suitable closure model for turbulence that a realistic flow prediction can be made. It should be emphasized, however, that the kinetic energy of turbulence results presented here must be viewed as qualitative. This is attributable to the fact that the additional production of turbulence energy by the rotational effects as well as the effects of blades curvature has been neglected in the present form of turbulence model.

Finally, the static temperature distribution within the blade-to-blade passage, nondimensionalized with respect to the inlet total temperature is given in Fig. 9. Inspection of

the contours plot indicates that the steepest gradients in temperature profiles occur near the blade suction surface at the channel inlet and near the pressure surface at the channel exit. This behavior is plausible, since the velocities in these regions are high (see Fig. 6). Conversely, it is observed that the thermal layers tend to thicken on the suction surface at trailing edge and also near the pressure surface where the recirculating zone exists. Since the rate of heat transfer to the blades is proportional to the temperature gradients near the surface, therefore, one can conclude that maximum rate of heat transfer occurs at the blade leading edge and also near the blade suction surface. This result has important impact on the process of designing the cooling passages for new impellers, particularly when the design procedure is based on specifying the blade temperature distribution. The present results suggest that in order to keep the blades cooled at constant temperature, it is necessary to place large number of cooling passages near the blade leading edge and also along the suction surface in the neighborhood of the impeller inlet.

5. CONCLUSIONS

A method has been developed which is suitable for analyzing the viscous flow within turbomachine passages. The field analysis was based upon the numerical integration of the full incompressible Navier-Stokes equations over a predetermined set of blade-to-blade stream surfaces. The method employs a nonorthogonal body-fitted coordinate system to account for the most complicated blade geometries. Effects of turbulence were modelled using a two-equation turbulence model.

Significant viscous flow results were obtained by applying the method of analysis to a radial inflow turbine. The predicted flow patterns indicated the severity of the complex interaction mechanism that occurs between the different flow regimes (i.e. boundary layers, recirculating eddies, separation zones, etc.). This result emphasized clearly the inaccuracies

involved in using a nonviscous flow solution with classical boundary layer techniques to obtain viscous flow details within turbomachine rotors. Heat transfer results pointed out that in order to keep the rotor blades cooled at uniform temperatures, it was necessary to place a large number of cooling passages near the blades leading edge and also along the suction surface in the vicinity of rotor inlet.

On the whole, it is recognized from the results presented here and in Volume I, that the present flow analysis provides a good prediction of the actual flow behavior within the passage of turbomachine rotors. This accomplishment cannot be attributed to any single element of the analysis, but results from the combinations of many factors. The major one is believed to be the preservation of the ellipticity of the problem by working with the full Navier-Stokes equations. Other important factors include the transformation, discretization and the numerical procedures used that provided stable calculations of good accuracy.

As with all research efforts of this magnitude, several areas for future work are recognized during the course of the present study. These include the use of variable grid in the numerical scheme, the inclusion of the effects of rotation and surface curvature in the turbulence model and the inclusion of the flow compressibility in the solution procedure. Similarly, the inaccuracies involved in using the present method to analyze flows including three dimensional separated zones are identified and documented (see Vol. I).

REFERENCES

1. Wu, C.H., "A General Theory of Three-Dimensional Flow in Subsonic and Supersonic Turbomachines of Axial, Radial and Mixed-Flow Types," National Advisory Committee for Aeronautics, TN 2604, 1952.
2. Stanitz, J.D., "Two-Dimensional Compressible Flow in Centrifugal Compressor," NACA TR 954, 1950.
3. Dodge, P.R., "A Numerical Method for 2-D and 3-D Viscous Flow," AIAA Paper No. 76-425, 1976.
4. Ribaut, M., "On the Calculation of Three-Dimensional Divergent and Rotational Flow in Turbomachines," Journal of Fluids Engineering, Vol. 99, Series 1, No. 1, pp. 187-196.
5. Sturge, D.P., "Compressible Flow in a Centrifugal Impeller with Separation, A Two-Dimensional Calculation Method," ASME Paper No. 77-WA/FE-8, 1977.
6. Thompson, J.F., Thames, F.C. and Wayne, C., "Automatic Numerical Generation of Body-Fitted Curvilinear Coordinate System for Field Containing Any Number of Arbitrary Two-Dimensional Bodies," Journal of Computational Physics, Vol. 15, 1974, pp. 299-319.
7. Khalil, I. and Tabakoff, W., "A Calculation Procedure for Viscous Flow in Turbomachines - Vol. I," NASA Report No. NASA CR 159635, July 1979.
8. Wilcox, D.C. and Chambers, T.L., "Critical Examination of Two-Equations Turbulence Closure Models," AIAA Paper No. 76-352, 1976.
9. Launder, B.E. and Spalding, D.B., "The Numerical Computations of Turbulent Flows," Computer Methods in Applied Mechanics and Engineering, Vol. 3, 1974, pp. 269-289.
10. Quemord, C. and Michel, R., "Definition and Application of Means for Predicting Shear Turbulent Flows in Turbomachines," ASME Paper 76-GT-67, 1976.
11. Khalil, I.M., Ph.D. Thesis, University of Cincinnati, 1978.
12. Hai, S.M., "Numerical Solution of Nonlinear Elliptic Partial Differential Equations by Successively Converging Techniques," Numerical/Laboratory Computers Methods in Fluid Mechanics, (an ASME publication).

NOMENCLATURE

A_1, A_2, A_5	Coefficients of the finite difference equations.
B_1, B_3, B_5	Coefficients of the finite difference equations.
b	Normal stream annulus thickness, m.
C_1, C_2, C_5	Coefficients of the finite difference equations.
$\bar{C}_1, \bar{C}_2, C_D$	Constants in the turbulence model.
C_p	Specific heat at constant pressure, J/(Kg)(°K).
D	Dissipation function.
D_1, D_2, D_5	Coefficients of the finite difference equations.
E	Kinetic energy of turbulence, J/Kg.
G_1, G_2, G_5	Denoting source terms in the flow governing equations.
h	Static enthalpy, J/Kg.
H	Total enthalpy, J/Kg.
J	Jacobian matrix.
K_1, K_2, K_5	Coefficients of the finite difference equations.
ℓ	Mixing length, m.
$\dot{M}$	Mass flow per blade flowing through the stream annulus, Kg/sec.
$\vec{n}$	Outward unit normal to the stream surface, S_1.
ΔN	Distance of the near-wall grid point (w+1) from the blade surface.
p	Static pressure, N/m^2 or blade pitch.
Pr	Effective turbulent Prandtl number.
r	Radius from axis of rotation, m.
R	Universal gas constant, U/(Kg)(°K).
Re	Reynolds number.
S_{CE}	Schmidt number for kinetic energy of turbulence.
$S_{C\varepsilon}$	Schmidt number for dissipation of kinetic energy of turbulence.
T	Temperature, °K.
$\bar{W}$	Relative velocity vector, m/sec.
W	Magnitude of $\bar{W}$, m/sec.
W_m	Meridional component of the relative velocity vector, m/sec.
W_ϕ	Tangential component of the relative velocity vector, m/sec.

x	Stretched meridional coordinate.
z	Axial coordinate, m.
Z	Number of blades.
α	Angle between m and z, rad., see Fig. 1.
β	Coordinate transformation parameter, or angle between relative velocity vector and meridional plane, rad., see Fig. 2.
γ	Coordinate transformation parameter.
δ	Coordinate transformation parameter.
ρ	Fluid density, Kg/m^3.
μ_e	Effective viscosity, m^2/sec.
μ_ℓ	Laminar viscosity, m^2/sec.
Ω	Rotational speed, rad/sec.
ϕ	Relative angular coordinate, rad.
ψ	Stream function.
ω	Vorticity, 1/sec.
ε	Dissipation of kinetic energy of turbulence, J/Kg.
ξ	Boundary fitted coordinate.
η	Boundary fitted coordinate.

Superscripts

-	Mean value.
*	Denotes nondimensional quantity.

Subscripts

e	Effective
ℓ	Laminar.
m	Meridional component
w	Wall value.
w+1	Pertaining to points in the flow field at a distance $\Delta\eta$ away from w.
ϕ	Tangential component.
i,j	Denotes field position in (ξ,η) domain, see Fig. 3b.
inlet	Inlet or upstream.
exit	Exit or downstream.
total	Total conditions.
t, tip	Rotor tip.

TABLE 1 - COEFFICIENTS OF THE FINITE DIFFERENCE EQUATIONS†

$$A_1 = 2\delta\ \Delta\eta/\Delta\xi/A_o/(b^*_{i+1} + b^*_i)$$

$$A_2 = 2\delta\Delta\eta/\Delta\xi/A_o/(b^*_{i-1} + b^*_i)$$

$$A_3 = \gamma\ \Delta\xi/\Delta\eta/A_o/b^*_i$$

$$A_4 = \gamma\ \Delta\xi/\Delta\eta/A_o/b^*_i$$

$$A_5 = \Delta\xi\ \Delta\eta\ \left[\frac{r_t}{r_o}\frac{b_t}{b_o}\omega^* R^2 J^2\ z/2\pi - \underline{\beta}\frac{\partial}{\partial\xi}\left(\frac{1}{b^*}\frac{\partial\psi}{\partial\eta}\right) - \underline{\beta}\frac{\partial}{\partial\eta}\left(\frac{1}{b^*}\frac{\partial\psi}{\partial\xi}\right)\right]/A_o$$

where

$$A_o = A_1 + A_2 + A_3 + A_4$$

† All unsubscript quantities in this table are evaluated at the grid node (i,j). Note that the stream channel thickness b^*_i is constant for all j.

TABLE 1 - CONTINUED

$$B_1 = [B_{11} + B_{12}\, b^*_{i+1}/(\tilde{Re})_{i+1,j}]\; b^*_i/b^*_{i+1} \quad , \qquad \tilde{Re} = \frac{r_o}{r_t}\,\frac{b_o}{b_t}\,\frac{2\pi}{z}\,Re$$

$$B_2 = [B_{21} + B_{22}\, b^*_{i-1}/(\tilde{Re})_{i-1,j}]\; b^*_i/b^*_{i-1}$$

$$B_3 = [B_{31} + B_{32}\, b^*_i/(\tilde{Re})_{i,j+1}]\; b^*_i/b^*_{i+1}$$

$$B_4 = B_{41} + B_{42}\, b^*_i/(\tilde{Re}_{i,j-1})$$

where

$$B_{11} = J(\psi_{11} + |\psi_{11}|)/8B_o$$

$$B_{12} = \delta\, \Delta\eta/\Delta\xi/B_o$$

$$B_{21} = J(\psi_{22} + |\psi_{22}|)/8B_o$$

$$B_{22} = \delta\, \Delta\eta/\Delta\xi/B_o$$

$$B_{31} = J(\psi_{33} + |\psi_{33}|)/8B_o$$

$$B_{32} = \gamma\, \Delta\xi/\Delta\eta/B_o$$

TABLE 1 - CONTINUED

$$B_{41} = J(\psi_{44} + |\psi_{44}|)/8B_o$$

$$B_{42} = \gamma\ \Delta\xi/\Delta\eta/B_o$$

$$B_5 = -\ 2\ \Delta\xi\ \Delta\eta\ b^*\left[\underline{\beta}\ \frac{\partial^2}{\partial\xi\ \partial\eta}\ \left(\frac{\omega^*}{\tilde{Re}}\right) + J\ \frac{R_o}{Re}\ \frac{\partial}{\partial\xi}\ \left(\frac{\sin\alpha}{b^*}\ \frac{\partial\psi}{\partial\eta}\right) + \frac{\partial}{\partial\eta}\ \left(\frac{\sin\alpha}{b^*}\ \frac{\partial\psi}{\partial\xi}\right)\right]/B_o$$

$$B_o = B_{11} + B_{21} + B_{31} + B_{41} + (B_{12} + B_{22} + B_{32} + B_{42})\ b^*/\tilde{Re}$$

$$\psi_{11} = \psi_{i+1,j-1} + \psi_{i,j-1} - \psi_{i+1,j+1} - \psi_{i,j+1}$$

$$\psi_{22} = \psi_{i-1,j+1} + \psi_{i,j+1} - \psi_{i-1,j-1} - \psi_{i,j-1}$$

$$\psi_{33} = \psi_{i+1,j+1} + \psi_{i+1,j} - \psi_{i-1,j+1} - \psi_{i-1,j}$$

$$\psi_{44} = \psi_{i-1,j-1} + \psi_{i-1,j} - \psi_{i+1,j-1} - \psi_{i+1,j+1}$$

TABLE 1 - CONTINUED*

$$C_1 = (C_{11} + C_{12})/C_o$$

$$C_2 = (C_{21} + C_{22})/C_o$$

$$C_3 = (C_{31} + C_{32})/C_o$$

$$C_4 = (C_{41} + C_{42})/C_o$$

where

$$C_{11} = J\, b_o^* \,(\psi_{11} + |\psi_{11}|)/8b^*$$

$$C_{12} = \delta\, \Delta\eta/\Delta\xi/Pr/[(\tilde{Re})_{i+1,j} + (\tilde{Re})_{i,j}]/2.0$$

$$C_{21} = J\, b_o^* \,(\psi_{22} + |\psi_{22}|)/8b^*$$

$$C_{22} = \delta\, \Delta\eta/\Delta\xi/Pr/[(\tilde{Re})_{i-1,j} + (\tilde{Re})_{i,j}]/2.0$$

* The Prandtl Number is assumed to be constant in this table.

TABLE 1 - CONTINUED

$$C_{31} = J\, b_o^{*}\, (\psi_{33} + |\psi_{33}|)/8b^{*}$$

$$C_{32} = \gamma\, \Delta\xi/\Delta\eta/Pr/[(\tilde{Re})_{i,j+1} + (\tilde{Re})_{i,j}]/2.0$$

$$C_{41} = J\, b_o^{*}\, (\psi_{44} + |\psi_{44}|)/8b^{*}$$

$$C_{42} = \gamma\, \Delta\xi/\Delta\eta/Pr/[(\tilde{Re})_{i,j-1} + (\tilde{Re})_{i,j}]/2.0$$

$$C_5 = \Delta\xi\, \Delta\eta\, [-D^{*} + G_4^{*} - \beta \frac{\partial}{\partial\xi} (\frac{1}{Re} \frac{1}{Pr} \frac{\partial H^{*}}{\partial\eta}) - \beta \frac{\partial}{\partial\eta} (\frac{1}{Re} \frac{1}{Pr} \frac{\partial H^{*}}{\partial\xi})]/C_o$$

$$C_o = C_{11} + C_{21} + C_{31} + C_{41} + (C_{12} + C_{22} + C_{32} + C_{42})$$

TABLE 1 - CONTINUED

$$D_1 = (D_{11} + D_{12})/D_o$$

$$D_2 = (D_{21} + D_{22})/D_o$$

$$D_3 = (D_{31} + D_{32})/D_o$$

$$D_4 = (D_{41} + D_{42})/D_o$$

where

$$D_{11} = J\ b_o^*\ (\psi_{11} + |\psi_{11}|)/8b^*$$

$$D_{12} = \delta\ \Delta\eta/\Delta\xi/S_{CE}/[(\tilde{Re})_{i+1,j} + (\tilde{Re})_{i,j}]/2.0$$

$$D_{21} = J\ b_o^*\ (\psi_{22} + |\psi_{22})|/8b^*$$

$$D_{22} = \delta\ \Delta\eta/\Delta\xi/S_{CE}/[(\tilde{Re})_{i-1,j} + (\tilde{Re})_{i,j}]/2.0$$

$$D_{31} = J\ b_o^*\ (\psi_{33} + |\psi_{33}|)/8b^*$$

$$D_{32} = \gamma\ \Delta\xi/\Delta\eta/S_{CE}/[(\tilde{Re})_{i,j+1} + (\tilde{Re})_{i,j}]/2.0$$

TABLE 1 - CONTINUED

$$D_{41} = J\, b_o^* \,(\psi_{44} + |\psi_{44}|)/8b^*$$

$$C_{42} = \gamma\, \Delta\xi/\Delta\eta/S_{CE}/[(\tilde{Re})_{i,j-1} + (\tilde{Re})_{i,j}]/2.0$$

$$D_5 = \Delta\xi\, \Delta\eta\, [-D^* + \frac{2\pi}{z} J^2 \varepsilon^* \frac{r^{*2}}{r_o} - \beta \frac{\partial}{\partial\xi} (\frac{1}{Re} \frac{1}{S_{CE}} \frac{\partial E^*}{\partial\eta}) - \beta \frac{\partial}{\partial\eta} (\frac{1}{Re} \frac{1}{S_{CE}} \frac{\partial E^*}{\partial\xi})]/D_o$$

$$D_o = D_{11} + D_{21} + D_{31} + D_{41} + (D_{12} + D_{22} + D_{32} + D_{42})$$

TABLE 1 - CONTINUED

$$K_1 = (K_{11} + K_{12})/K_o$$

$$K_2 = (K_{21} + K_{22})/K_o$$

$$K_3 = (K_{31} + K_{32})/K_o$$

$$K_4 = (K_{41} + K_{42})/K_o$$

where

$$K_{11} = J\, b_o^* (\psi_{11} + |\psi_{11}|)/8b^*$$

$$K_{12} = \delta\, \Delta\eta/\Delta\xi/S_{C\varepsilon}/[(\tilde{Re})_{i+1,j} + (\tilde{Re})_{i,j}]/2.0$$

$$K_{21} = J\, b_o^* (\psi_{22} + |\psi_{22}|)/8b^*$$

$$K_{22} = \delta\, \Delta\eta/\Delta\xi/S_{C\varepsilon}/[(\tilde{Re})_{i-1,j} + (\tilde{Re})_{i,j}]/2.0$$

$$K_{31} = J\, b_o^* (\psi_{33} + |\psi_{33}|)/8b^*$$

$$K_{32} = \gamma\, \Delta\xi/\Delta\eta/S_{C\varepsilon}/[(\tilde{Re})_{i,j+1} + (\tilde{Re})_{i,j}]/2.0$$

TABLE 1 - CONTINUED

$$K_{41} = J\, b_o^* (\psi_{44} + |\psi_{44}|)/8b^*$$

$$K_{42} = \gamma\, \Delta\xi/\Delta\eta/S_{C\varepsilon}/[(\tilde{Re})_{i,j-1} + (\tilde{Re})_{i,j}]/2.0$$

$$K_5 = \Delta\xi\, \Delta\eta\, [-\bar{C}_1\, D^*\, \frac{\varepsilon^*}{E^*} + \frac{z}{2\pi}\, \bar{C}_2\, J^2\, \frac{\varepsilon^{*2}}{E^*}\, \frac{r^{*2}}{r_o} - \beta\, \frac{\partial}{\partial\xi}\, (\frac{1}{Re}\, \frac{1}{S_{C\varepsilon}}\, \frac{\partial\varepsilon^*}{\partial\eta}) - \beta\, \frac{\partial}{\partial\eta}\, (\frac{1}{Re}\, \frac{1}{S_{C\varepsilon}}\, \frac{\partial\varepsilon^*}{\partial\xi})]/K_o$$

$$K_o = K_{11} + K_{21} + K_{31} + K_{41} + (K_{12} + K_{22} + K_{32} + K_{42})$$

TABLE 2: BLADE GEOMETRY DATA RADIUS

Blade Lower Surface Data

Meridional Distance m(m)	Angular Coordinate ϕ	Derivative	2nd Derivative
0.62539D-03	0.56273	-0.45678	-7.2554
0.86000D-02	0.55900	-0.46035	6.3594
0.16000D-01	0.55560	-0.43120	-11.995
0.23500D-01	0.55220	-0.35261	46.288
0.29030D-01	0.55050	-0.34501	-43.542
0.34280D-01	0.54900	-0.52816D-01	154.86
0.39540D-01	0.54640	-1.7845	-813.31
0.46230D-01	0.51540	-7.6118	-928.77
0.53940D-01	0.42600	-15.982	-1242.5
0.61970D-01	0.23650	-33.844	-3206.4
0.67011D-01	0.23898D-01	-50.743	-3497.8

Blade Upper Surface Data

Meridional Distance m(m)	Angular Coordinate ϕ	Derivative	2nd Derivative
0.62539D-03	0.84710D-02	0.45678	5.7000
0.86000D-02	0.12200D-01	0.46655	-3.2487
0.16000D-01	0.15600D-01	0.45729	0.74568
0.23500D-01	0.18900D-01	0.40262	-15.325
0.29030D-01	0.20900D-01	0.32213	-13.787
0.34280D-01	0.21500D-01	-0.26520	-209.96
0.39540D-01	0.16000D-01	-2.0543	-470.30
0.46230D-01	-0.11600D-01	-8.6949	-917.03
0.53940D-01	-0.96200D-01	-15.993	-1495.0
0.61970D-01	-0.27910	-30.342	-0278.9
0.68363D-01	-0.53070	-50.743	-4303.7

TABLE 2: BLADE GEOMETRY DATA

Meridional Distance m(m)	Radius from Center of Rotation	sinα	Stream Annulus Thickness, b(m)
-0.007079	0.083527	-1.004280	0.000967
-0.003684	0.080123	-1.000120	0.000956
0.0	0.076450	-0.993984	0.000960
0.003498	0.072986	-0.985732	0.000982
0.006853	0.069697	-0.974760	0.001013
0.010048	0.066603	-0.960602	0.001043
0.013104	0.063701	-0.937357	0.001068
0.016034	0.060999	-0.904973	0.001090
0.018845	0.058511	-0.862745	0.001110
0.021535	0.056258	-0.810406	0.001128
0.024127	0.054236	-0.749061	0.001144
0.026630	0.052443	-0.681938	0.001156
0.029055	0.050874	-0.610477	0.001160
0.031413	0.049519	-0.540900	0.001155
0.033711	0.048348	-0.478504	0.001157
0.035959	0.047338	-0.420336	0.001179
0.038162	0.046477	-0.360370	0.001216
0.040329	0.045762	-0.299578	0.001253
0.042466	0.045177	-0.250202	0.001284
0.044574	0.044690	-0.214878	0.001310
0.046662	0.044266	-0.192922	0.001335
0.048730	0.043881	-0.180691	0.001362
0.050782	0.043516	-0.176406	0.001389
0.052817	0.043155	-0.179872	0.001416
0.054835	0.042782	-0.190020	0.001441
0.056835	0.042392	-0.200095	0.001465
0.058816	0.041987	-0.208736	0.001490
0.060776	0.041570	-0.215980	0.001514
0.062717	0.041145	-0.220585	0.001540
0.064639	0.040729	-0.209999	0.001568
0.066544	0.040353	-0.181434	0.001595
0.068434	0.040051	-0.135325	0.001620
0.070308	0.039843	-0.088592	0.001642
0.072176	0.039709	-0.057745	0.001660
0.074039	0.039618	-0.042105	0.001673
0.075898	0.039550	-0.031892	0.001681
0.077754	0.039499	-0.023363	0.001686
0.079607	0.039462	-0.016506	0.001688

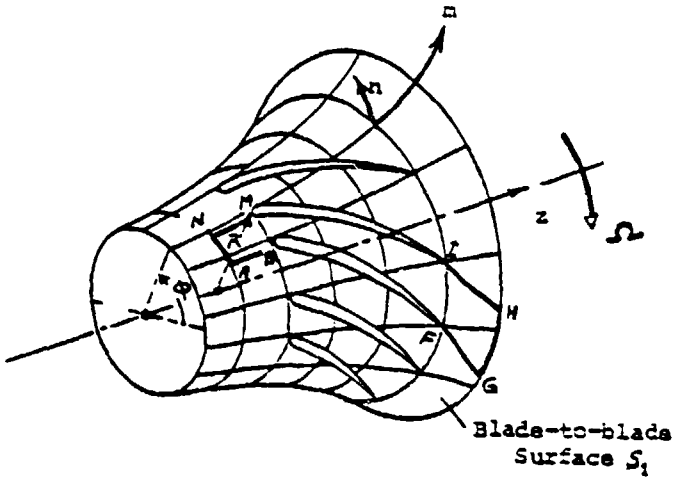

a) BLADE ROW INTERSECTION WITH A STREAM SURFACE.

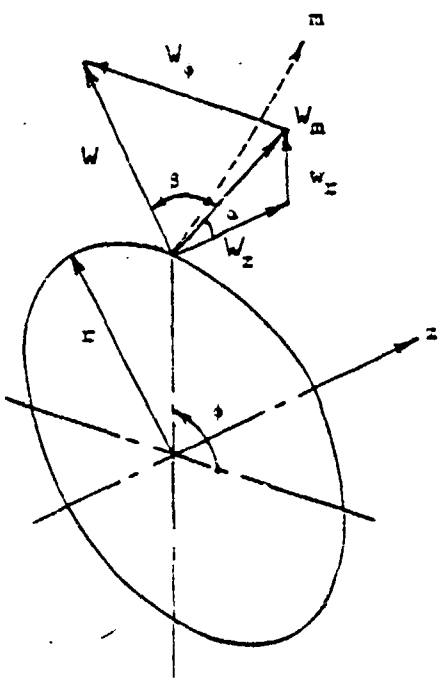

b) COORDINATE SYSTEM AND VELOCITY COMPONENTS.

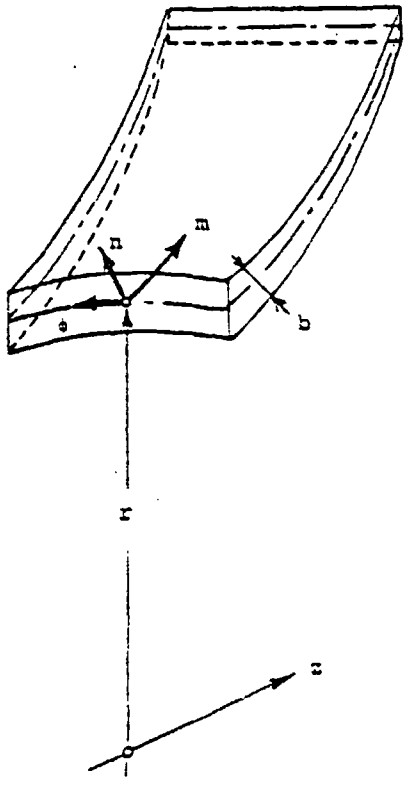

c) DETAILS OF STREAM SURFACE COORDINATE SYSTEM WITH FINITE THICKNESS SHEET.

FIG. 1. BLADE-TO-BLADE STREAM SURFACE S_1.

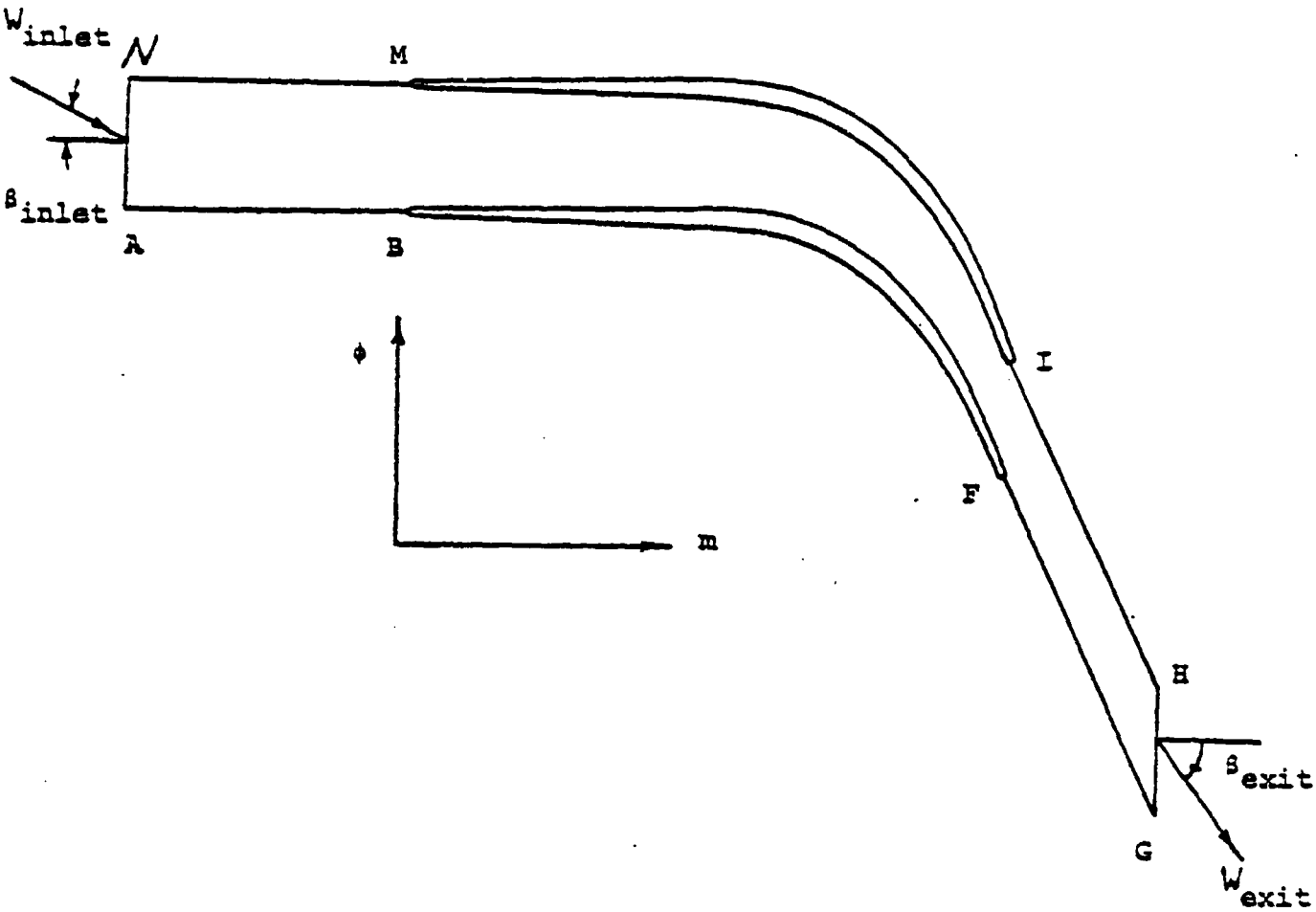

FIG. 2 . COMPUTATIONAL DOMAIN IN THE PHYSICAL SPACE.

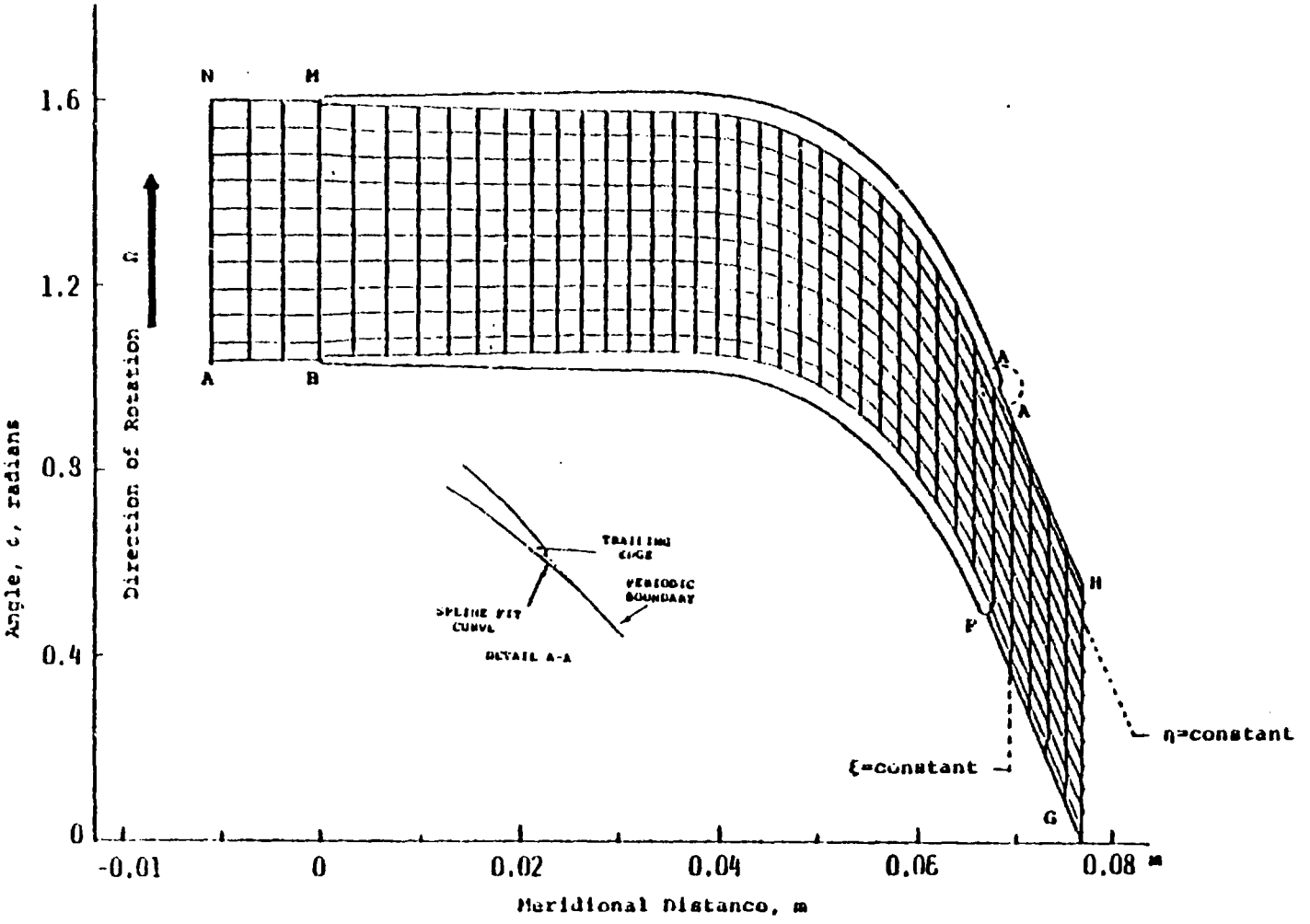

FIG. 3A. BOUNDARY FITTED COORDINATE SYSTEM.

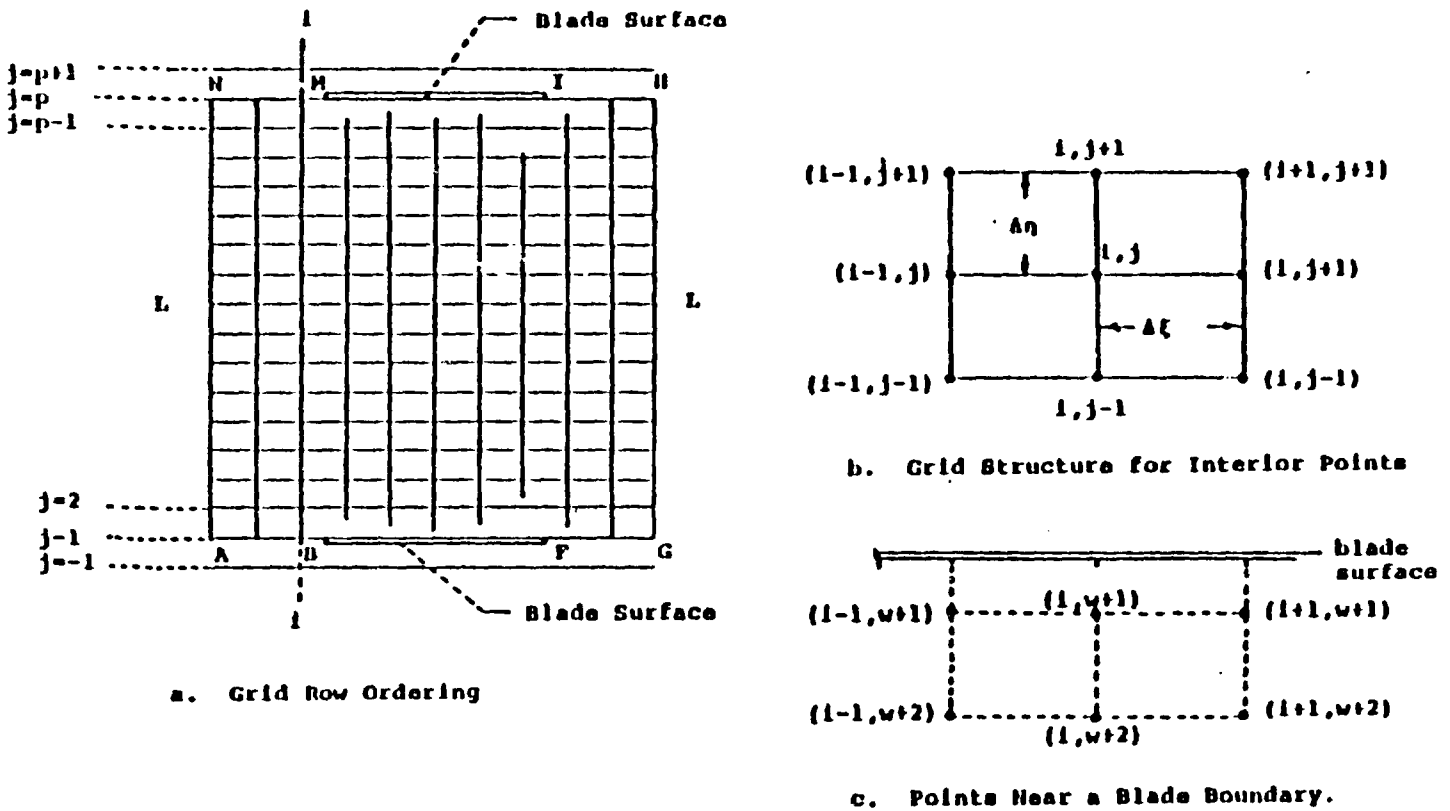

FIG. 3B. GRID ORDERING SYSTEM IN THE TRANSFORMED DOMAIN.

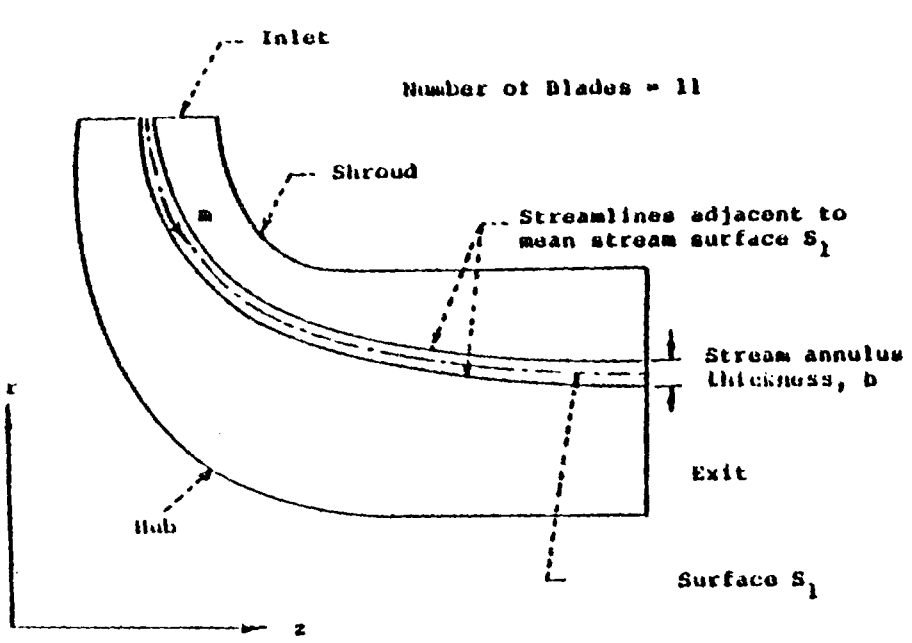

a. Meridional View

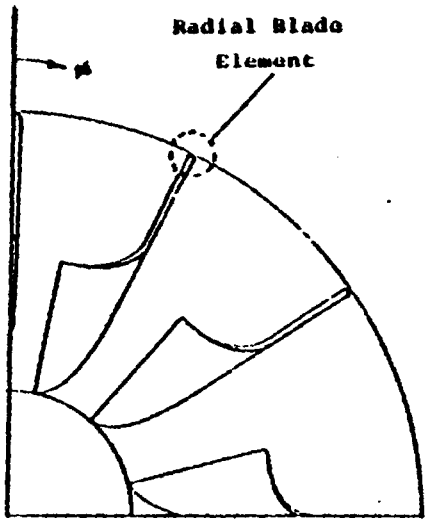

b. Blade-to-Blade View (Schematic)

FIG. 4. HUB-SHROUD PROFILE WITH STREAM SURFACE S_1, USED FOR BLADE-TO-BLADE ANALYSIS.

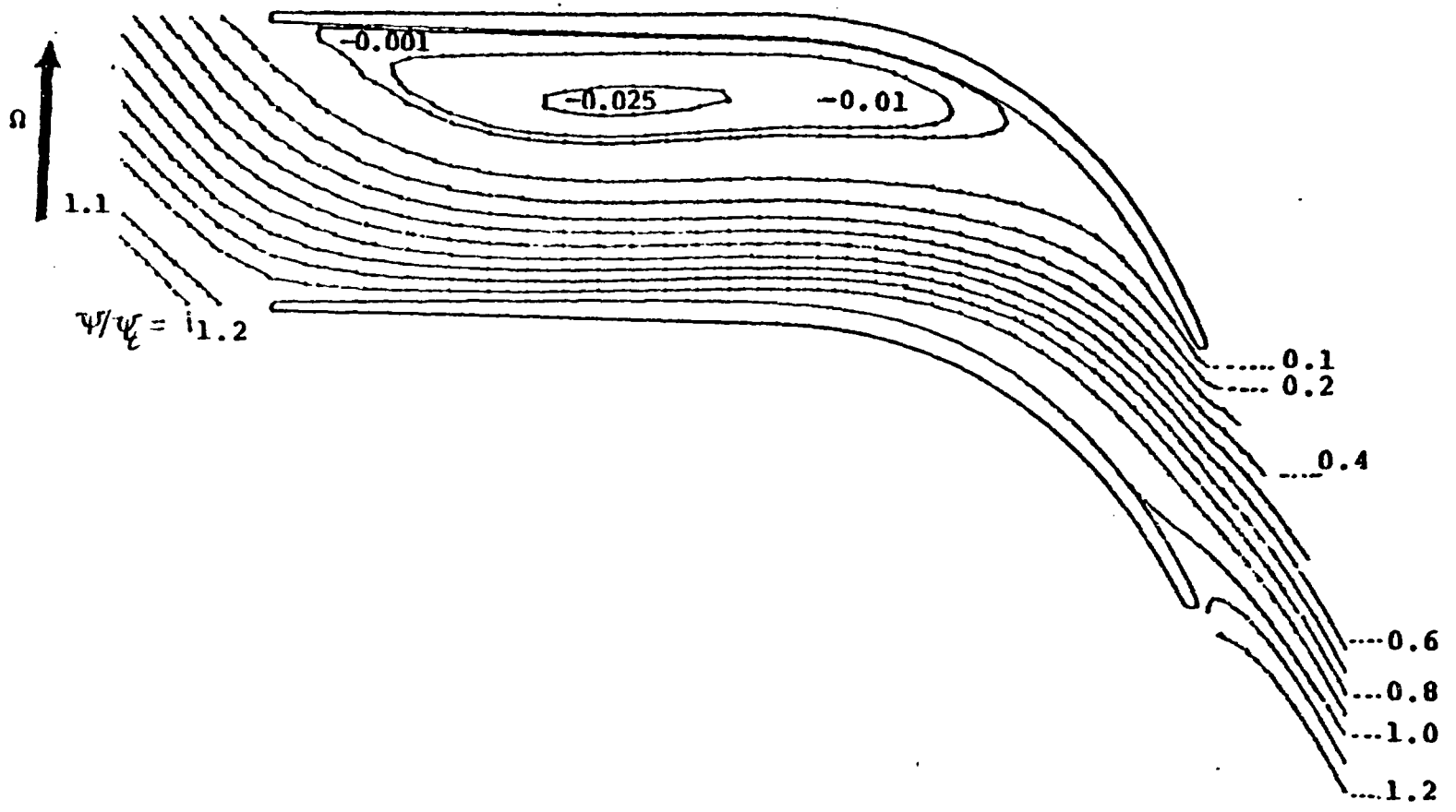

FIG. 5. RELATIVE STREAMLINES ψ/ψ_t.

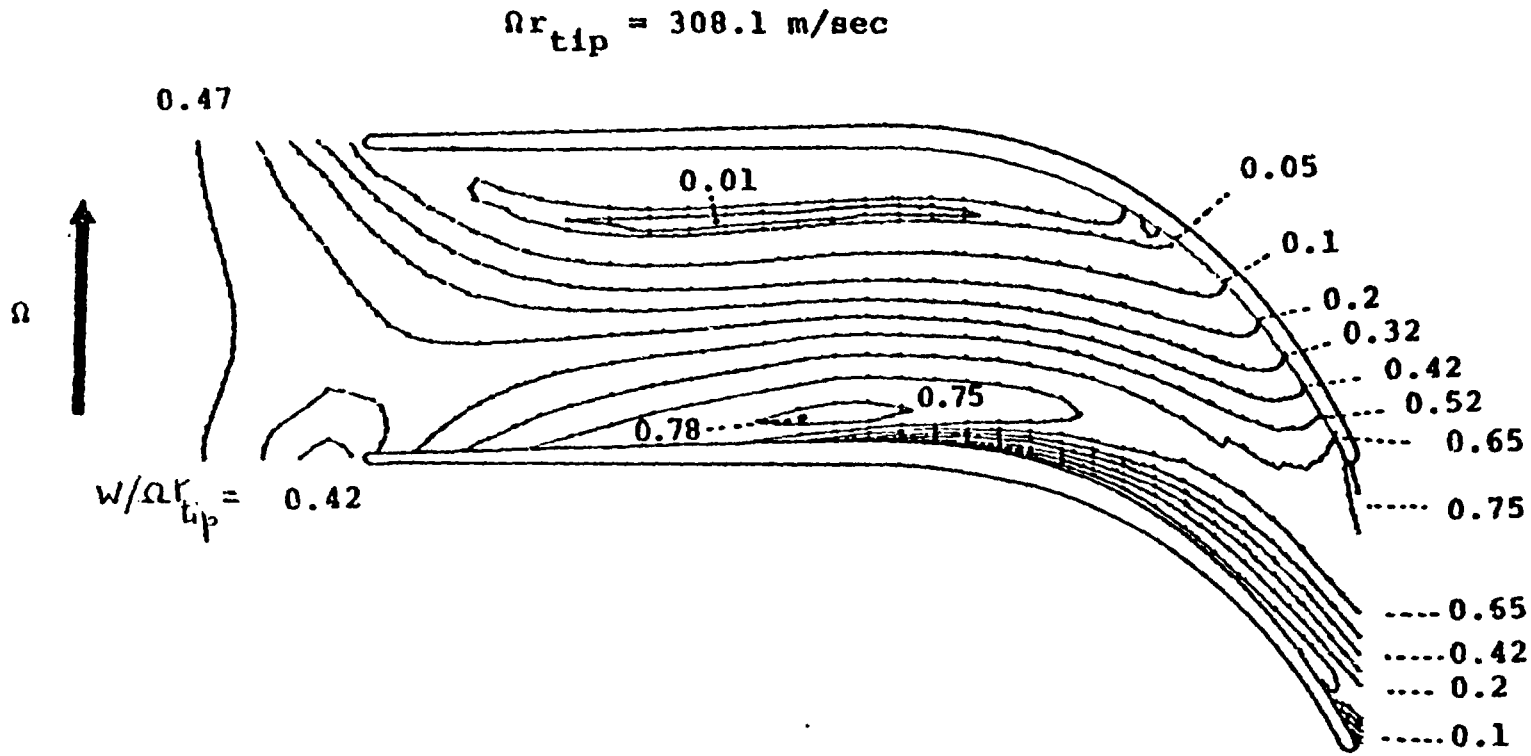

FIG. 6 RELATIVE VELOCITY DISTRIBUTION $(W/\Omega r_{tip})$

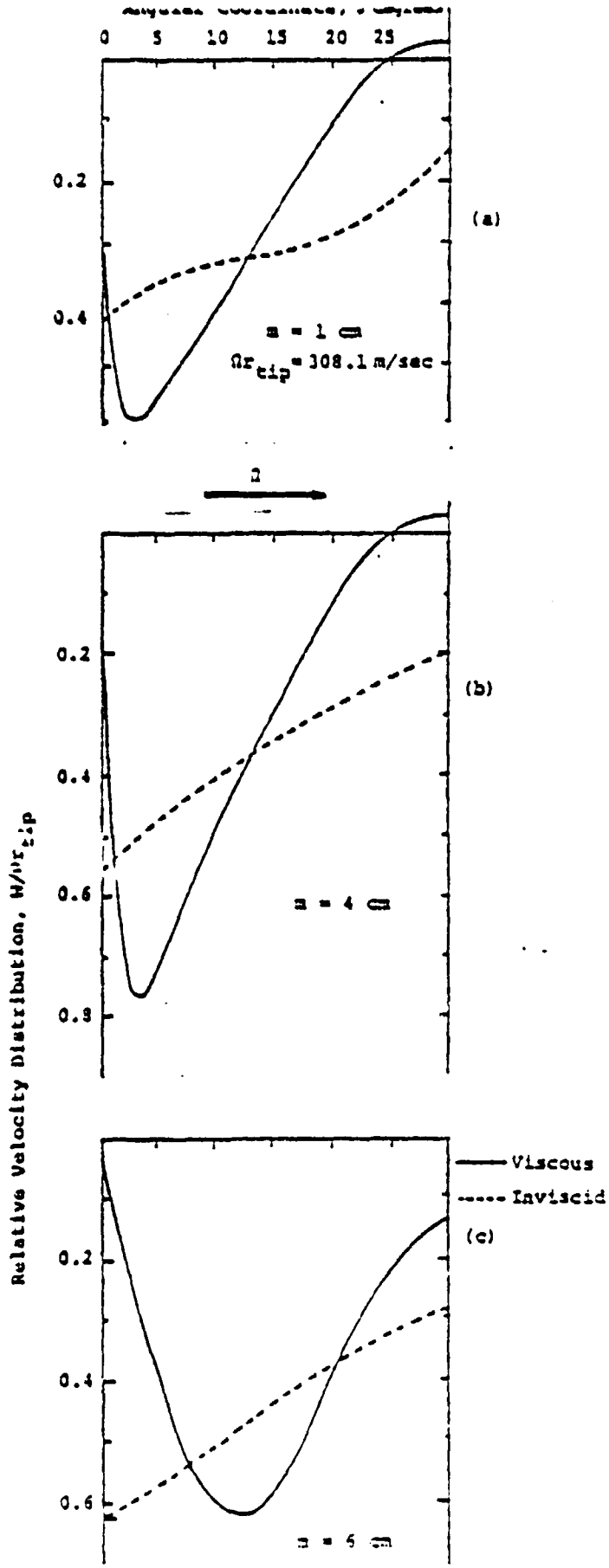

FIG. 7. NONDIMENSIONAL VELOCITY DISTRIBUTION AT DIFFERENT MERIDIONAL LOCATIONS.

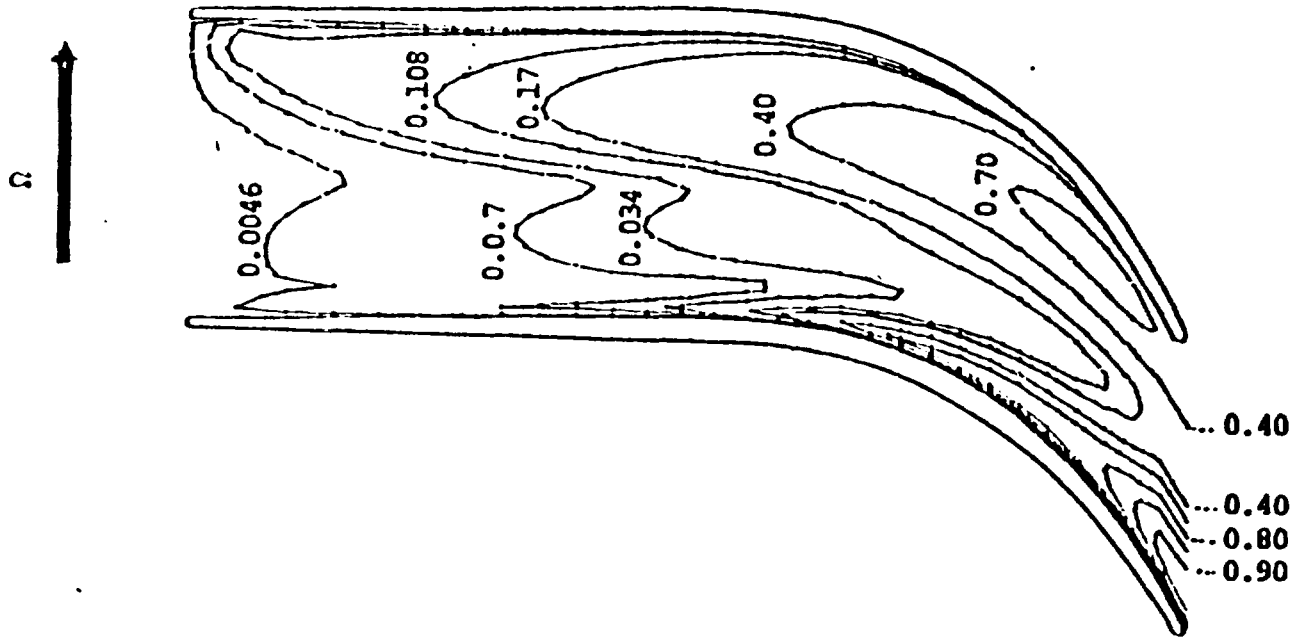

FIG. 8 KINETIC ENERGY OF TURBULENCE DISTRIBUTION $[(E/\Omega^2 r_{tip}^2) \times 10^2]$

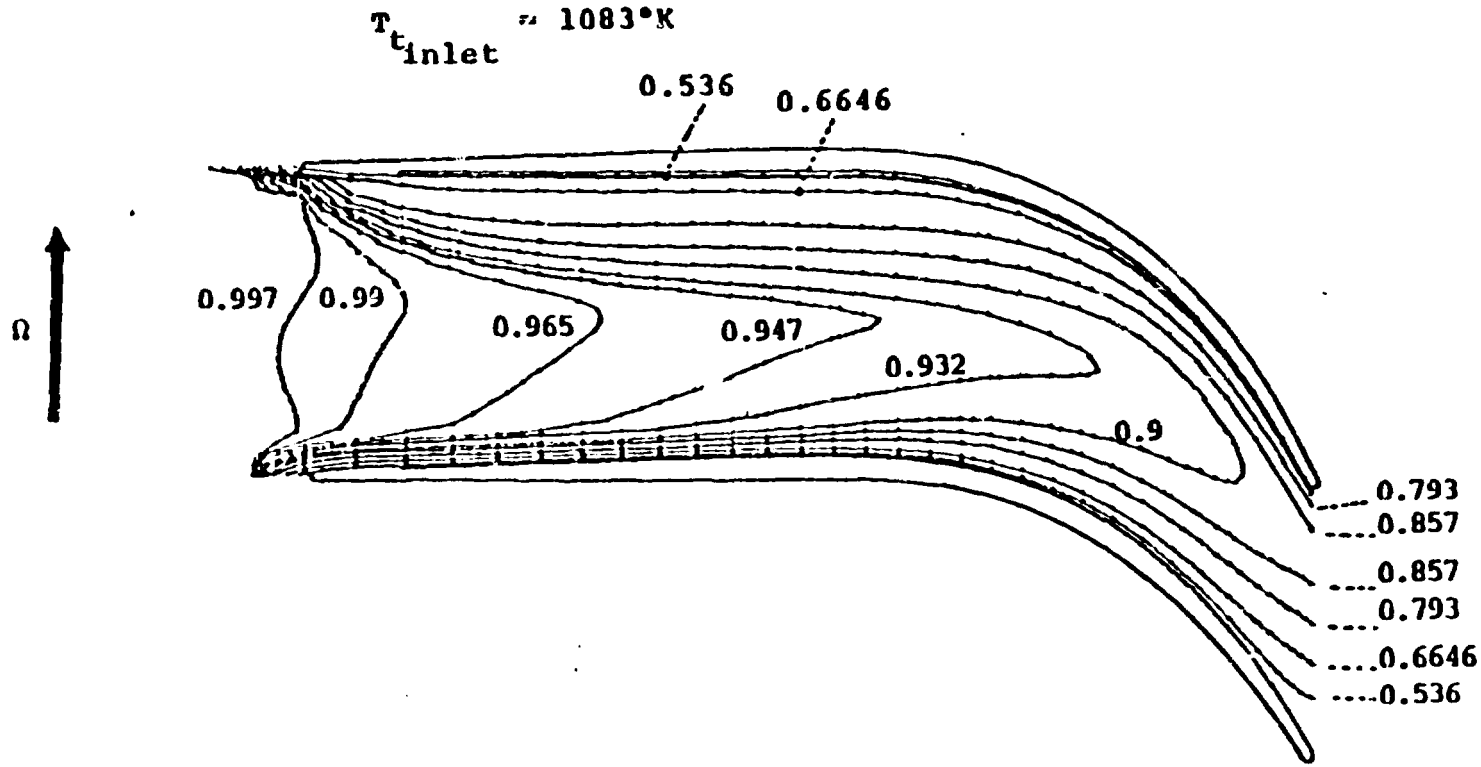

FIG. 9. TEMPERATURE DISTRIBUTION $(T/T_{t_{inlet}})$